Advances in Reliability, Safety and Security, Part 7 – Kołowrocki, Magryta-Mut (eds.)
 ISBN 978-83-68136-19-7 (printed), ISBN 978-83-68136-06-7 (electronic)

Advances in Reliability, Safety and Security

ESREL 2024
Monograph Book Series

Research Of Multi-Scale Failure Behavior Of Through-Silicon Via Under Thermal Cycling Load Based On Crystal Plastic Finite Element Method

Kaihong Hou, Zhengwei Fan, Xun Chen, Shufeng Zhang, Yashun Wang, Yu Jang

National University of Defense Technology, Laboratory of Science and Technology on Integrated Logistics Support, College of Intelligence Science and Technology, Changsha, China

Abstract

The through-silicon via (TSV) is widely adopted to achieve vertical connection between each chip and plays an important role in 3D packaging technology, while its failure mechanisms under thermal cycling needs to be further revealed. In the current study, the thermal expansion behavior and microstructure evolution of TSV under thermal cycling load is studied based on crystal plastic finite element method (CPFEM) where the temperature-related crystal plastic parameters and thermal expansion coefficients are introduced. Results reveal that under thermal cycling load, the stress-strain of Cu column is higher than that in silicon and silicon dioxide and the interleaved stated streaks of strain contour image is caused by the slip and interaction of slip systems. Scale effect of TSV is determined by both the continuous reduction TSV dimeter and the different cumulative shear strain distributions among different slip systems, and the maximum and minimum cumulative shear strain are observed in slip system (111) $[\bar{1}10]$ and $(1\bar{1}1)$ [011] respectively. Thermal cycling load has more influence on the thermal expansion of TSV than the evolution of orientation. the mean Cu grain area increases from 55.42 μm^2 to 65.74 μm^2 after thermal cycling, while the dispersion of grain area decreases significantly.

Keywords: through-silicon via (TSV), crystal plastic finite element method (CPFEM), temperture-dependence, cumulative shear strain

1. Introduction

With the advent of the intelligent era, the high-performance electronic devices are increasing demand, advanced electronic packaging especially 3D packaging technology has appeared and attracted wide attention (Chen, 2021; Lancaster, 2019). As the essential interconnected microstructure, the through-silicon via (TSV) is widely adopted to achieve vertical connection between each chip, which can not only shorten the connection length and improve the connection density in the chip, which brings the advantages of low delay, high bandwidth, low power consumption, small size and high performance, but also provides the possibility for the heterogeneous integration of MEMS and microelectronics chips. Therefore, the TSV-based 3D packaging is called “beyond Moore” packaging technology for it breaking of many limitations of two-dimensional chips.

The traditional TSV consists of a silicon substrate, an insulating layer, an isolating layer, a filling material, and a redistribution layer, and seed layer should be introduced if the plating process is used. TSV microstructure is a typical multi-material and multi-interface microstructure, its dimensions are generally from a few microns to about 100 microns, and the scale from chip package to TSV spans multiple scales. When the size of the TSV decreased to about 100 μm, the size of Cu grain will even approach that of TSV after annealing, which results in the filling material presents strong anisotropy, so the influence of crystal plasticity and grain boundary movement becomes non-negligible. The scale effect is very obvious in micro- and nano-chip devices, while current evaluation methods of the reliability of micro and nano chip devices are often derived from the reliability analysis based on macroscopic electronic products, and ignore the change of performance degradation, failure mechanism and failure mode caused by scale effect. Therefore, the reliability analysis of TSV should not only consider the macroscopic mechanical behavior, but also pay attention to the evolution characteristics of

microstructures. Electron Backscatter Diffraction (EBSD) is a technique used to analyze the textures of materials and characterize grain size and boundaries. Song et al. applied the EBSD technique to investigate the microstructure evolution of Cu under different annealing temperatures (Song, 2019). Zare et al. study the protrusion behavior of TSV during thermal annealing (Zare, 2020). Although EBSD technique is an effective technique to characterize microstructure evolution, but it is extremely costly, time-consuming and has certain limitations, therefore, the crystal plastic finite element method (CPFEM) comes into being and has been widely used. Based on the crystal plasticity theory, researches like fatigue damage (Liu, 2019), martensitic phase transformation (Park, 2019) and material forming (Hippke, 2020) are carried out. Raabe et al. (2007) and Cereceda et al. (2017) conducted crystal plastic finite element analysis of single crystal copper and single crystal tungsten based on CPFEM, which provided inspiration for the application of CPFEM to the failure mechanism analysis of TSV microstructure. Kumar et al. (2017) simulated the grain microstructure evolution of filler materials under thermal cycling through CPFEM and found that large shear stress generated along grain boundaries could drive grain boundary sliding (Sonawane, 2021) and copper crystal texture would affect copper expansion. These studies provide valuable reference for the failure analysis of TSV, but the crystal plastic parameters adopted by most of the studies are constant, which has great limitations for the investigation of the failure mechanism of TSV that is often used in the thermal cycle load environment.

In this study, the thermal expansion behavior of TSV under thermal cycling load is studied by introducing temperature-related crystal plastic parameters and considering the thermal expansion coefficients of Cu, silicon and silicon dioxide, and the failure behavior and microstructure evolution of TSV is studied from the dimensions of macro-scale stress and strain to micro-scale grain orientation and cumulative shear strain of slip system, which can provide some reference for the failure mechanism analysis of TSV.

2. Establishment of crystal plasticity constitutive model

2.1. Kinematics for crystal plasticity

The rate-dependent constitutive relies on the multiplicative decomposition of the total deformation gradient referred to the undeformed crystal configuration, F, into an inelastic component F^p and an elastic component F^e:

$$F = F^e F^P \tag{1}$$

where F^e accounts for the elastic stretching and rigid-body rotations, and F^P associated with dislocation slip while the lattice remains undistorted and unrotated. From the kinematics of dislocation motion, rate of the inelastic deformation gradient is given as:

$$\dot{F}^p F^{p-1} = \sum_\alpha \dot{\gamma}^\alpha P_0^\alpha \tag{2}$$

$$P_0^\alpha = m_0^\alpha \otimes n_0^\alpha \tag{3}$$

where $\dot{\gamma}^\alpha$ is the slip rate in a slip system α, m_0^α and n_0^α are the slip direction and the unit normal vector of slip plane in the reference configuration, respectively. The velocity gradient in the current state is:

$$L = \dot{F}F^{-1} = D + \Omega \tag{4}$$

where D was the symmetric part of L, representing the rate of stretching, and Ω the antisymmetric part of L, representing the spin rate. D and Ω can also be decomposed into an elastic part and a plastic part as follows:

$$D = D^e + D^p, \Omega = \Omega^e + \Omega^p \tag{5}$$

2.2. Constitutive laws for crystal plasticity

Based on the research of Huang (Huang, 1997) about the single crystal plasticity, the resolved shear strain rate $\dot{\gamma}^\alpha$ can be regard as the power function of the current strength g^α and resolved shear stress τ^α on slip system α:

$$\dot{\gamma}^\alpha = \dot{a}\left(\left|\frac{\tau^\alpha}{g^\alpha}\right|\right)^n sign\left(\frac{\tau^\alpha}{g^\alpha}\right) \tag{6}$$

where $\dot{a}$ is the reference strain rate, it's the value in this study is set as 0.001, and n is the rate sensitivity parameter. Based on the Schmid's law, the relation between resolved shear stress τ^{α} and stress σ can be described as:

$$\tau^{\alpha} = \sigma : \mu^{\alpha} \tag{7}$$

where μ^{α} is the Schmid factor, which can be expressed by the vectors normal to the slip plane (m_i^{α} and m_j^{α}) and the slip direction (s_i^{α} and s_j^{α}) in the slip system α :

$$\mu_{ij}^{\alpha} = \frac{1}{2}\left[s_i^{\alpha} m_j^{\alpha} + s_j^{\alpha} m_i^{\alpha} \right] \tag{8}$$

The evolution of slip system strength $\dot{g}^{\alpha}$ is determine by the isotopic hardening, and can be described by:

$$\dot{g}^{\alpha} = \sum_{\beta} h_{\alpha\beta} \left| \dot{\gamma}^{\beta} \right| \tag{9}$$

where $h_{\alpha\beta}$ is the hardening moduli, indicating the yield stress increment caused by the shear strain increment of β slip system, and $\dot{\gamma}^{\beta}$ is the resolved shear strain rate on slip system β . The model introduced in this study:

$$h_{\alpha\alpha} = h(\gamma) = h_0 \operatorname{sech}^2 \left| \frac{h_0 \gamma}{\tau_s - \tau_0} \right| (no\ sum\ on\ \alpha) \tag{10}$$

$$h_{\alpha\beta} = qh(\gamma)(\alpha \neq \beta) \tag{11}$$

where h_0 is the initial hardening modulus, and its value is set as 800 MPa. τ_s is the saturation stress and τ_0 is the initial value of slip system's strength. The ratio of latent hardening to self-hardening is defined as q, and its value for the FCC metals is set as 1.

In this study, crystal plasticity constitutive parameters are derived from the study of Lei et al (Lei, 2022), in which Young's modulus E, rate sensitivity parameter n, initial strength on slip system g_0 and the saturation stress τ_s are temperature-related, detailed value can be expressed by (12) to (15).

$$\tau_s = -0.1978T + 292.54 \tag{12}$$

$$g_0 = -0.1577T + 215.67 \tag{13}$$

$$n = -0.0011T + 2.3366 \tag{14}$$

$$E = -39.668T + 97361 \tag{15}$$

The crystal plastic constitutive is realized by the subroutine of Abaqus UMAT, the basic function realization can be referred to Huang's research (Huang, 1997). The macroscopic mechanical parameters of copper, silicon and silicon dioxide represented by typical through-silicon holes are shown in Table 1.

Table 1. Material properties adopted in the FEA mode.

Material	Si	SiO_2	Cu
	162000, 273 K		
Young's Modulus (MPa)	150000, 323 K	60100	UMAT
	140000, 373 K		
Poisson's ratio	0.23	0.16	0.3
			1.52E-05, 200 K
Thermal expansion coefficient (mm/K)	6E-7	6E-7	1.67E-05, 300 K
			1.75E-05, 400 K

3. Construction of CPFE model

3.1. Voronoi tessellation

In this study, the reconstruction of Cu grains is based on the non-weighted Voronoi tessellation (Voronoï, 1908), which associates each point in the domain uniquely to the nearest neighboring seed-point. To generate an m-dimensional, non-weighted Voronoi tessellation in space χ , n seed-points, $p^k(x)$, with coordinates x are

randomly distributed based on RSA algorithm. The morphology of the Voronoi cells is depended on the distribution of the distance between seed-points, and the point set is described as:

$$P = \left\{ p^1, ..., p^n \right\} \subset \mathbb{R}^m \tag{16}$$

where $2 \le n \le \infty, x^k \ne x^l$ for $k \ne l$ and $k, l \in I_n = \{1, ..., n\}$. Then the m-dimensional Voronoi polytope based on p^k can be written as:

$$X(p^k) = \left\{ x \mid \left\| x - x^k \right\| \le \left\| x - x^l \right\| \text{ for } k \ne l, k, l \in I_n \right\} \tag{17}$$

The corresponding set of polytopes can be described as:

$$\chi(p) = \left\{ X(p^1), ..., X(p^n) \right\} \tag{18}$$

Then a closed, periodic Voronoi diagram is obtained. The field of application of such a tessellated space ranges from single-phase grain arrangements where a crystallographic orientation is assigned to the individual grains or to study two or multiphase grain arrangements by assigning different phase-specific properties to selected grains.

3.2. TSV Construction

In this study, the Cu grains of TSV is reconstructed by python script based on Voronoi tessellation theory, and then the corresponding finite element model is created in Abaqus though running python script. The established TSV model is shown as Fig. 1. The TSV model consists of 120 Cu grains, SiO_2 layer and Si substrate, the specific geometric dimensions of TSV model are recorded in Table 2. TSV model is mesh by CPS4R element, and the TSV model contains 29516 elements. The three degrees of freedom of the bottom edge of TVS model are restricted, and the degrees of freedom in the X direction of the two sides of the TSV model are restricted. To simulate the thermal cyclic loading, a predefined field is applied with initial temperature of 298 K, the maximum and the minimum temperature are set as 423 K to 233 respectively, the temperature increment and the total calculation time are selected as 500 K/s and 1 second.

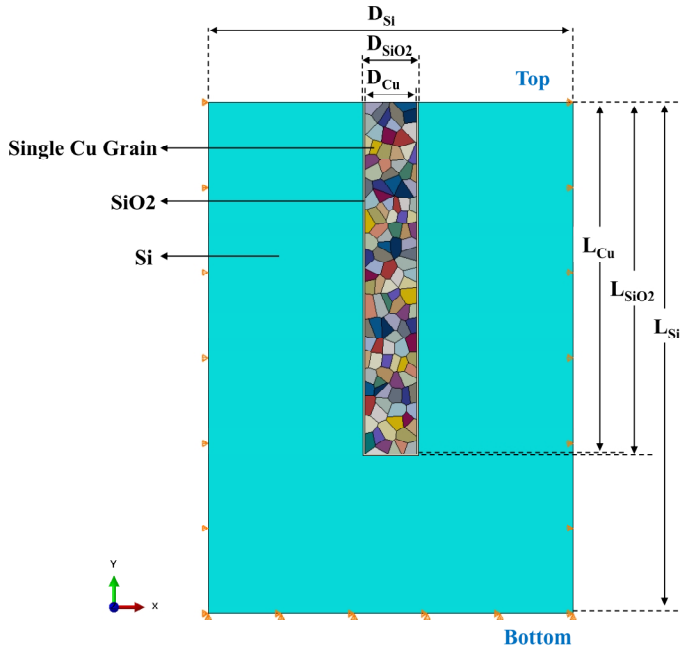

Fig. 1. TSV model created by python script.

Based on the finite element model of TSV, the EBSD file can be constructed, and then can be processed by MATLAB plug-in MTEX (Hielscher, T, 2022), so more microscope information of TSV microstructure can be obtained, likes orientation density distribution (ODF), misorientation distribution, grain area distribution, grain boundary information and so on. The EBSD map of TSV under initial state is shown as Fig. 2a, and Fig. 2b is the orientation of Cu based on EBSD map, more information results can be obtained from Fig. 2. Based on the orientation data, the grain boundary can be restructure, and the TSV FEM model can be further generate by MTEX. In this study, the Si and SiO2 are treated as isotropic material, and the orientation of Cu grains are assigned with random orientation.

Table 2. Specific geometric dimensions of TSV model.

Items	Value	Items	Value
L_{Cu}	200μm	D_{Cu}	30μm
L_{SiO2}	201μm	D_{SiO2}	32μm
L_{Si}	291μm	D_{Si}	212μm

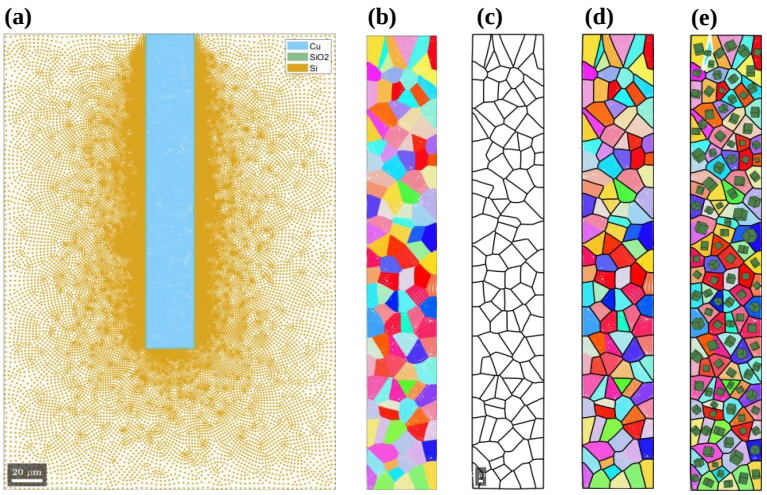

Fig. 2. Micro information acquisition process based on MTEX: (a) EBSD map of TSV; (b) orientation of Cu grains based on EBSD map; (c) grains reconstruction; (d) FEM model based on MTEX; (e) Cu grains FEM model with different orientation.

4. Results and discussions

4.1. Mechanics property analysis of TSV

Fig. 3 describes the mises stress and logarithmic strain distribution of Cu column, an obvious outburst phenomenon of Cu can be observed, it is mainly caused by the thermal mismatch between Cu, silicon and silicon dioxide under the action of thermal cycle load. Compared with silicon and silicon dioxide, the stress and strain inside Cu column are larger, and the dispersion of stress and strain are more obvious, which is consistent with the phenomenon obtained by Lei et al. (Lei, 2022). Compared with the traditional study based on Cu being isotropic material, this study reveals the phenomenon of stress concentration and stress non-uniform distribution at the interface between Cu column and silicon dioxide, as well as at the Cu grain boundary. As can be seen from the Fig. 3a, the maximum and the minimum mises stress are 376.1 MPa and 105.7 MPa respectively, corresponding to the stress range of 270.4 MPa. There are also great differences in strain, with the maximum logarithmic strain of 0.02339 and the minimum of 0.002801. It is interesting that some obvious streaks of 45 degrees can be observed from the strain contour image, and these streaks present interleaved state. The interesting phenomenon is most likely caused by the slip of the slip systems and the interaction of slip systems. The activation of the slip system arises a high strain value around grain boundary, thus the strain peak value can be obviously obtained from Fig. 3b.

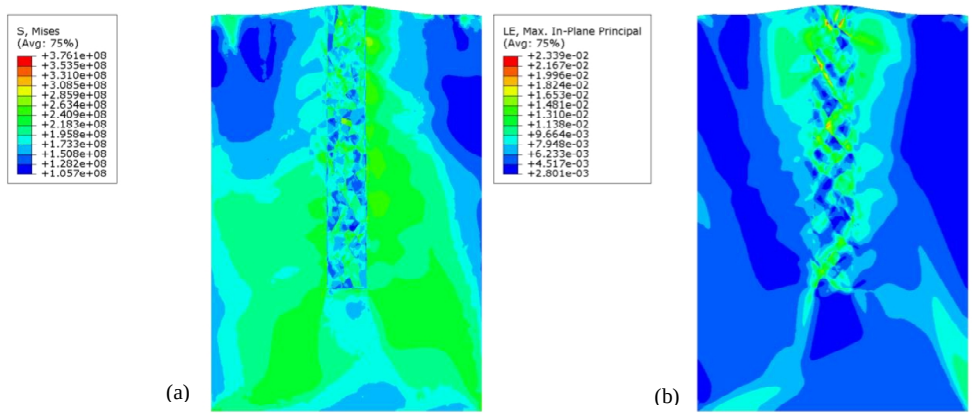

Fig. 3. Stress-strain distribution among TSV: (a) Stress distribution; (b) Strain distribution.

Fig. 4 has recorded the cumulative shear strain distribution of 12 slip system. It can be found that the cumulative shear strain distribution of each slip system is different, the maximum cumulative shear strain is in slip system $(111)\ [\bar{1}10]$, the minimum cumulative shear strain is located in slip system $(1\bar{1}1)\ [011]$. Under the action of circulating thermal load, most of Cu grains are suffered thermal expansion, resulting in the bulging phenomenon of Cu grains, while some Cu grains are compressed by other grains, which expand under the thermal load, that is why some negative value of cumulative shear strain can be found in the cloud map. The existence of grain boundaries can block the flow deformation of material, then a serious cumulative shear strain will be generated near the grain boundaries, which is consistent with the cumulative shear strain distribution at B1, B2 and B3 labeled in Fig. 4. To characterize the influence of shear slip of different slip systems on the plastic deformation of TSV, the maximum cumulative shear strain and cumulative shear strain range of 12 slip systems are introduced as characterization parameter. Herein agreed that the greater the maximum cumulative shear strain, the greater the contribution of cumulative shear strain generated by the current slip system to TSV plastic deformation, and that the greater the cumulative shear strain range, the scale effect is present more strongly on current slip system. From results of Fig. 5, some conclusions can be obtained that the largest contribution to the deformation of TSV is slip system $(111)\ [\bar{1}10]$, followed by system $(\bar{1}11)\ [0\bar{1}1]$, and the smallest is system $(1\bar{1}1)\ [011]$. The scale effect is most obvious in slip system $(\bar{1}11)\ [\bar{1}10]$, followed by $(\bar{1}11)\ [0\bar{1}1]$, and the one with the least scale effect corresponds to slip system $(1\bar{1}1)\ [011]$. Based on the analysis above, some novel conclusions can be found that the scale effect of TSV is due to the continuous reduction of its size on the one hand, and the different cumulative shear strain distributions produced by different slip systems on the other hand, which provides a new perspective for us to understand the scale effect of TSV.

It can be observed from Fig. 6 that the orientation distribution of Cu grains does not change greatly after suffered thermal cycling load, only one worth mentioning is some of the orientation has been weakened. In general, the influence of the thermal cycle load on the orientation distribution is not obvious, which can be explained as the results of the rotation of the grains is masked by their thermal expansion effect. The phenomenon can be further confirmed by the area distribution of grains. It can be seen from Fig. 7 that after thermal cycling, the mean grain area increases from 55.42 μm^2 to 65.74 μm^2, and the dispersion of grain area also decrease significantly, which may be due to the fusion and migration of grain boundaries under the thermal cycle load.

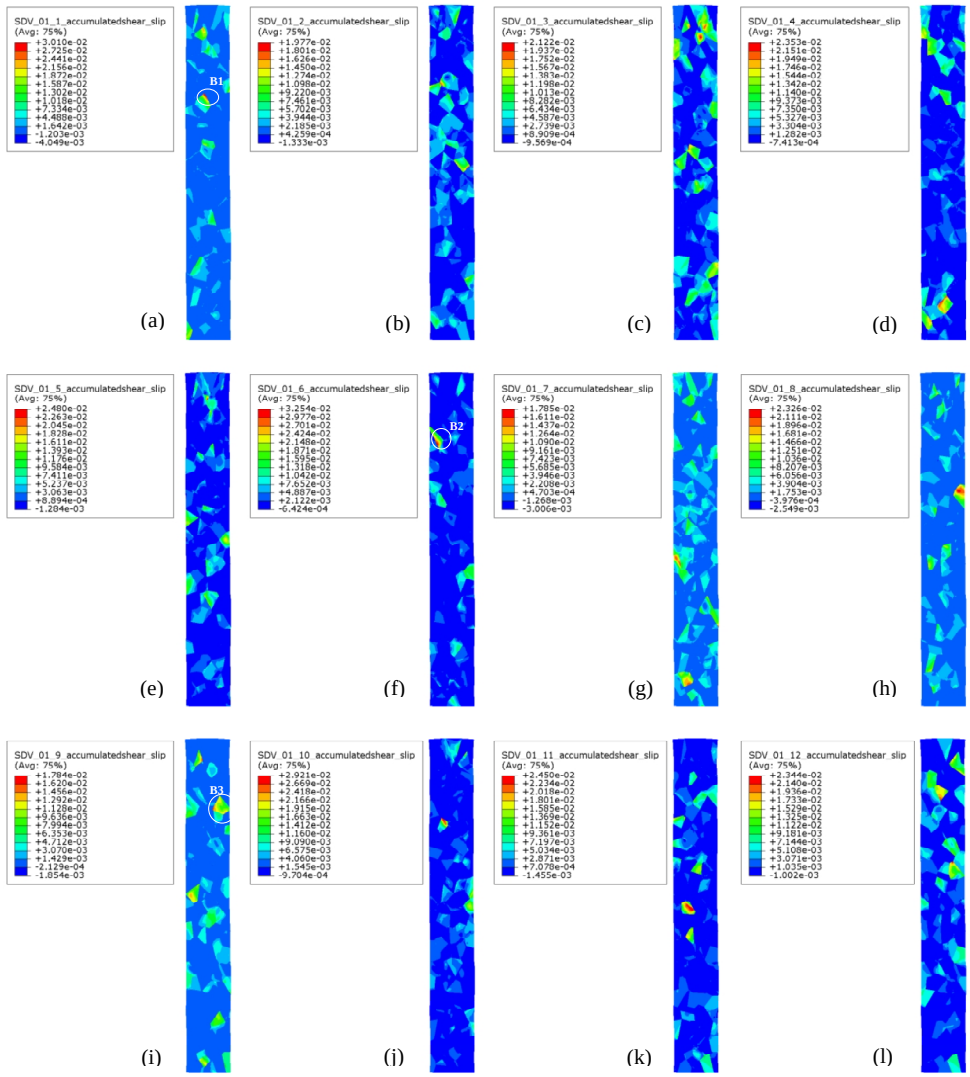

Fig. 4. Cumulative shear strain distribution among Cu column within different slip system:
(a) (111) [-110]; (b) (111) [-101]; (c) (111) [01-1]; (d) (-111) [110]; (e) (-111) [101]; (f) (-111) [101];
(g) (-111) [0-11]; (h) (1-11) [110]; (i) (1-11) [-101]; (j) (1-11) [011]; (k) (11-1) [101]; (l) (11-1) [011];.

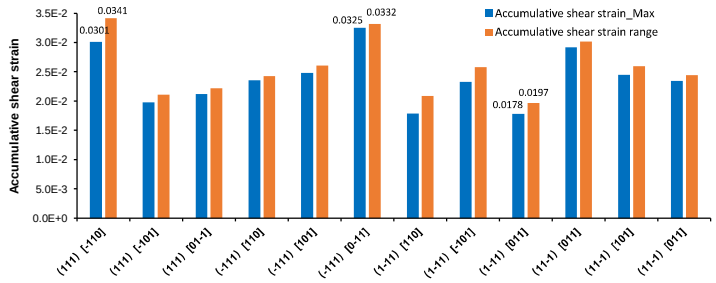

Fig. 5. Corresponding maximum cumulative shear strain and cumulative shear strain range under different slip systems.

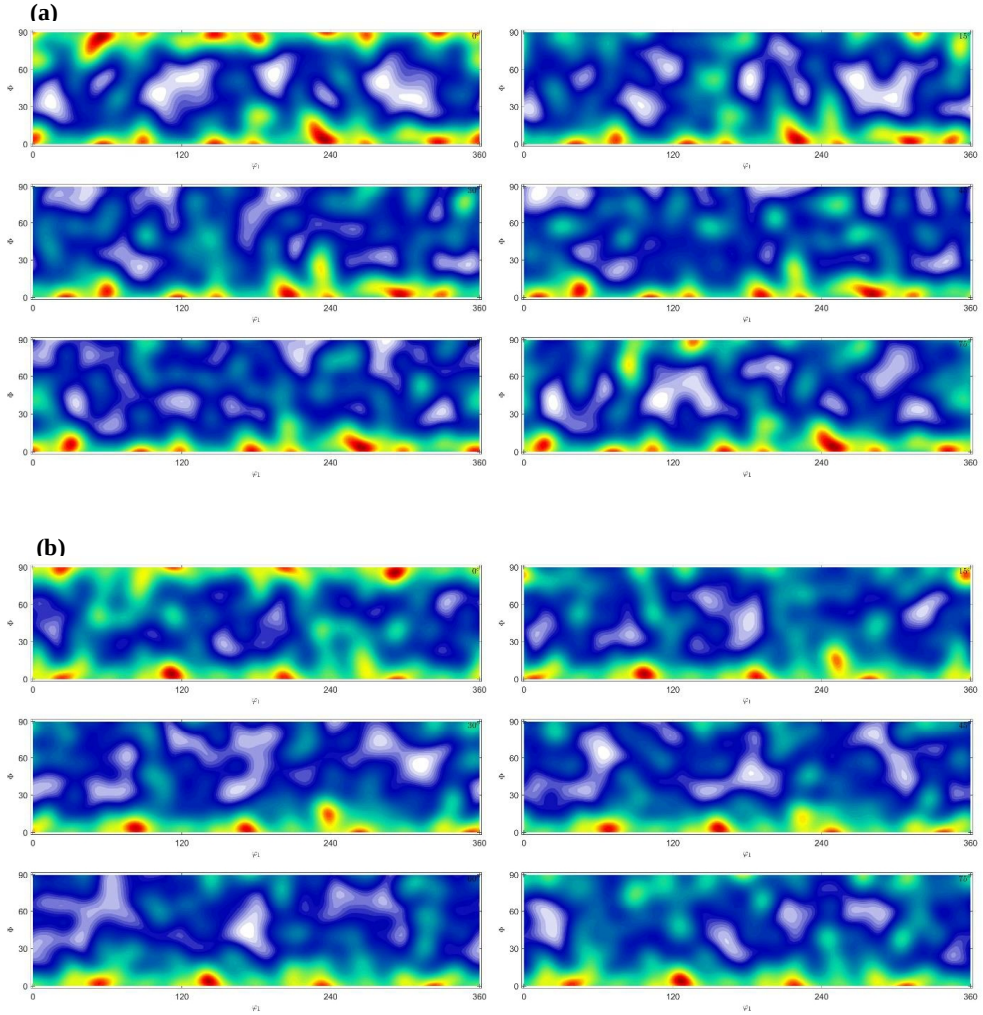

Fig. 6. ODF. (a) before thermal cycle, after; (b) after thermal cycle.

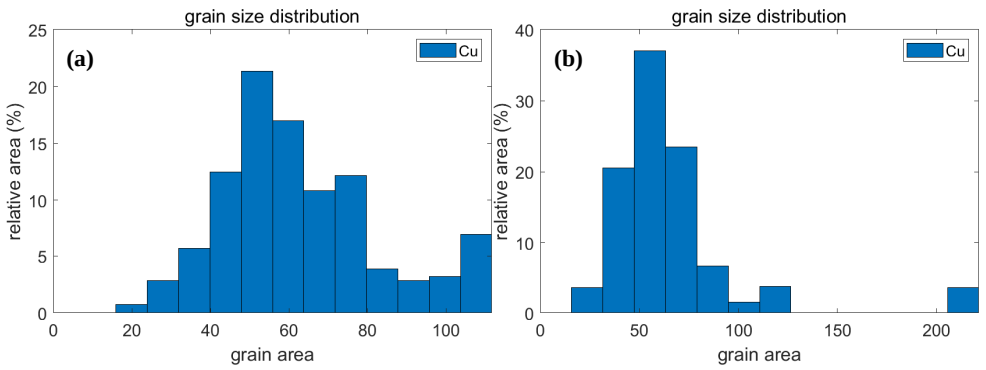

Fig. 7. Grain size distribution. (a) before thermal cycle, after; (b) after thermal cycle.

5. Conclusions

In this study, the thermal expansion behavior of TSV under thermal cycling load is studied based on crystal plastic finite element method, here the crystal plastic parameters and thermal expansion coefficients are defined as temperature-related. The microstructure evolution of TSV is studied from the dimensions of macro-scale stress and strain to micro-scale grain orientation and cumulative shear strain of slip system. From the analysis, the following conclusions can be drawn: (1) Compared with silicon and silicon dioxide, the stress-strain of Cu column is higher and the stress-strain dispersion is larger. The strain contour image of Cu presents obvious interleaved stated streaks of 45 degrees, which is most likely caused by the slip and interaction of slip systems; (2) The maximum and minimum cumulative shear strain are observed in slip system $(111)[\bar{1}10]$ and $(1\bar{1}1)[011]$ respectively. The scale effect of TSV is determined by both the continuous reduction TSV dimeter and the different cumulative shear strain distributions among different slip systems. (3) Thermal cycling load has more influence on the thermal expansion of TSV than the evolution of orientation. After thermal cycling, the mean Cu grain area increases from 55.42 μm^2 to 65.74 μm^2, and the dispersion of grain area also decrease significantly.

Acknowledgements

This research work is sponsored by the National Natural Science Foundation of China (No. 52275166), Youth Independent Innovation Science Fund of NUDT (ZK23-29), National Key Laboratory Fund and Hunan Graduate Research Innovation Project (CX20230020).

References

Cereceda, D., Dilehl, M. 2017. Unraveling the temperature dependence of the yield strength in single-crystal tungsten using atomistically-informed crystal plasticity calculations. International Journal of Plasticity 78, 242-65.

Chen, Y., Xie, B. 2021. Interfacial laser-induced graphene enabling high-performance liquid− solid triboelectric nanogenerator, Advanced Materials 33 (44), 2104290.

Hielscher, R., Nyyssönen, T. 2022. The variant graph approach to improved parent grain reconstruction. Materialia 22, 101339.

Hippke, H., Hirsiger, S. 2020. Optimized and validated prediction of plastic yielding supported by cruciform experiments and crystal plasticity, International Journal of Material Forming 13, 841-852.

Huang, Y. A User-material Subroutine Incroporating Single Crystal Plasticity in the ABAQUS Finite Element Program, Harvard Univ, Cambridge, 1991.

Kumar, P., Dutta, I. 2017. Microstructural and Reliability Issues of TSVSpringer International Publishing. 71-99.

Lancaster, A., Keswani, M.. 2018. Integrated circuit packaging review with an emphasis on 3D packaging. Integration 60, 204–212.

Lei, M., Wang, Y. 2022. Microstructure evolution and mechanical behavior of copper through-silicon via structure under thermal cyclic loading. Microelectronics Reliability.

Liu, L., Wang, J. 2019. Crystal plasticity model to predict fatigue crack nucleation based on the phase transformation theory, Acta Mechanica Sinica 35, 1033-1043.

Park, T., Hector, L.G. 2019. Crystal plasticity modeling of 3rd generation multi-phase AHSS with martensitic transformation. International Journal of Plasticity 120, 1-46.

Raabe, D., Ma, D. 2007. Effects of initial orientation, sample geometry and friction on anisotropy and crystallographic orientation changes in single crystal microcompression deformation: A crystal plasticity finite element study. Acta Materialia 55 (13), 4567-83.

Sonawane, D., Kumar, P. 2021. Role of Grain Boundary Sliding in Structural Integrity of Cu-Filled Through Si Via During Isothermal Annealing. Journal of Electronic Materials 50, 767-778.

Song, M., Wei, Z. 2019. Study on copper protrusion of through-silicon via in a 3-D integrated circuit, Materials Science and Engineering: A 755 (7), 66-74.

Voronoï, G. 1908. Nouvelles applications des paramètres continus à la théorie des formes quadratiques. Deuxième mémoire.Recherches sur les parallèlloédres primitifs. Journal für Die Reine Und Angewandte Mathematik 134, 198-287.

Zare, Y., Sasajima, Y. 2020. A novel lining method for eliminating plastic deformation and protrusion of copper in cu-TSV using FEM analysis. Journal of Electronic Materials 49, 3692-3700.